An alternative representation of the receptance: the 'elliptical plane' and its modal properties.

Diogo Montalvão[a*], *Daerefa-a Mitsheal Amafabia*[b]

[a] Department of Design and Engineering, Faculty of Science and Technology, Bournemouth University, Poole House, Talbot Campus, Fern Barrow, Poole BH12 5BB, United Kingdom
[b] School of Engineering and Technology, University of Hertfordshire, College Lane Campus, Hatfield AL10 9AB, United Kingdom

ABSTRACT

Modal Identification from Frequency Response Functions (FRFs) has been extensively investigated up to the point its research reached a stagnation state. Yet, a new approach to determine the modal damping factors from FRFs was recently proposed, showing that there still is scope for new findings in the field. Contrary to other modal identification methods which are based on the dynamic motion governing equations, the method used the dissipated energy per cycle of vibration as a starting point. For lightly damped systems with conveniently spaced modes, it produced quite accurate results, especially when compared to the well-known method of the inverse. The method used a plot of the sine of the phase of the receptance against its amplitude, whereby damping was determined from the slope of a linear fit to the resulting plot. In this paper, it is shown that this plot has other (perhaps more important) special properties that were not explored before. Near resonant frequencies, its shape is elliptical, whereby the real and imaginary parts of the modal constants can be determined from numerical curve-fitting. This finding allowed developing a new method which formulation is presented in this paper. The method is discussed through numerical and experimental examples. Although the intention is not to present a new modal identification method that is superior to other existing ones (like the method of the inverse or those based on the Nyquist plot), the authors believe that this new representation of the receptance and its properties may bring valuable insights for other researchers in the field.

Keywords: experimental modal analysis (EMA); modal identification; modal constants; dissipated energy; elliptical plane.

1. Introduction

The interest of modal identification procedures is acknowledged by the scientific community and many authors have addressed this problem, mainly since the early seventies of the past century [1]. The existing to date modal identification procedures cover different levels of sophistication and, in almost all cases, require the use of software that may not be easy to obtain.

In the past few years, attention has been more focused on Operational Modal Analysis (OMA) rather than in the more traditional Experimental Modal Analysis (EMA). Examples of later developments in OMA identification methods can be found, for instance, in [2-5]. In terms of EMA, later publications are more concerned with Engineering applications or dealing with uncertainty in existing methods, as

[*] Corresponding author. Tel.: +44(0)1202 965513.

E-mail address: dmontalvao@bournemouth.ac.uk.

can be seen, for instance, in [6, 7]. OMA deals with operational deflection shapes and many often make use of output-only measurements, this meaning that excitation loads are unknown. EMA makes use of both input forces and output responses in order to determine modal parameters and mode shapes. Numerous modal identification algorithms have been developed in the past thirty years [8]. However, even if in the past recent years not many advances have been seen in terms of EMA modal identification methods, there are a few interesting results that can still be derived.

If the sole objective is the determination of the global modal characteristics, it is possible to use simple approaches that produce quick estimates of the desired information. The issue of determining the modal damping factors has recently been presented [9, 10] from a different perspective. In that new approach, the starting point was the dissipated energy per cycle of vibration rather than the governing equations of the dynamic motion as it is usually done. The proposed methodology is based on a special plot of the receptance, whereby the vertical axis is the sine of the phase angle and the horizontal axis is the amplitude (in a similar fashion to what is done with the Nyquist plot of the receptance).

As it is shown in this paper, this plot has special properties, one of which is that the data points around a resonant frequency describe a loop that resembles the half of an ellipse. It is also shown that the major and minor axis of the ellipse are related to the modal constants, which can be determined using numerical extrapolation methods. Modal constants are important because they contain information about the mode shapes (local modal characteristics) which, in the general case of non-proportional damping, are complex quantities [1]. Modal identification techniques seek to extract from experimental data the modal parameters that characterise the dynamic behaviour of a structure [11]. Thus, a modal model is derived through the determination of the values (for each mode of vibration) of the natural frequency (not explored in this paper), damping ratio (explored in [9, 10]) and complex modal constant (explored in this paper). Once the modal model is known, it can be used in many different fields of structural dynamics, e.g., structural modification, coupling techniques (including mass cancelation), finite element updating, transmissibility and structural health monitoring, just to mention a few [1, 12-18].

This paper presents the development of the new proposed methodology for the determination of the modal constants and illustrates its application through both numerical and experimental examples. It is important to note that the intention is not to present a new approach to modal identification that is superior to existing ones (like the method of the inverse or those based on the Nyquist plot). However, the fact that this new representation of the receptance in an 'elliptical plane' is a function of the modal properties, is a reason for the authors to believe that this research may bring valuable insights to other researchers in the field.

2. Theoretical development

The development presented in sections 2.1 and 2.2 is not original and has been previously presented in detail in [10]. However, the authors considered it would be important to summarise it here so that the whole of the proposed method can be better understood.

2.1. Definitions

Let us start from the well-known second-order differential equation of motion for a single degree of freedom (SDOF) viscous system given by:

$$m\ddot{x} + c\dot{x} + kx = Fe^{i\omega t} \tag{1}$$

where m is the mass, c is the viscous damping coefficient, k is the stiffness, F is the amplitude of the oscillatory force, t is the time variable and $i = \sqrt{-1}$ is the imaginary number. When excited by an harmonic force at a frequency ω, it can be easily proven (and most fundamental texts on vibration theory show it, for instance [1, 14]) that for each vibration cycle the system dissipates – through its

viscous damper – a quantity of energy directly proportional to the damping coefficient, the excitation frequency and the square of the response amplitude X:

$$W_{diss} = \int_0^T f\dot{x}ht = \pi c\omega X^2 \tag{2}$$

where $T = 2\pi/\omega$ is the time period of oscillation. However, experimental evidence from tests performed on a large variety of materials show that the damping due to internal friction (material hysteresis) is nearly independent of the forcing frequency but still proportional to the square of the response amplitude [19], i. e.:

$$W_{diss} \propto CX^2 \tag{3}$$

where C is a constant. Therefore, from equations (2) and (3) the equivalent damping coefficient is:

$$c = \frac{C}{\pi\omega} = \frac{h}{\omega} \tag{4}$$

where h is the hysteretic damping coefficient. In such conditions, equation (1) can be re-written as:

$$m\ddot{x} + \frac{h}{\omega}\dot{x} + kx = Fe^{i\omega t} \tag{5}$$

If the stiffness is a complex quantity, i.e., defined as the sum of the stiffness itself (k, real part) and the damping coefficient (h, imaginary part):

$$k^* = k + ih = k(1 + i\eta) \tag{6}$$

where

$$\eta = h/k \tag{7}$$

and knowing that $\dot{x} = i\omega x$ for harmonic motion, equation (5) may be re-written as:

$$m\ddot{x} + k(1 + i\eta)x = Fe^{i\omega t} \tag{8}$$

The latter formulation (8) leads to the conclusion that the dissipated energy per cycle of vibration is independent of the forcing frequency.

2.2. Determination of the hysteretic damping

The experimental measurement of the hysteretic damping factor can be carried out by means of cyclic force-displacement tests in the elastic domain [20]. Following the reasoning presented earlier, it is easy

to show that the energy dissipated per cycle of oscillation is given by the ellipse area of the force-displacement plot during a complete cycle. Rearrangement of equations (2), (4) and (7) lead to:

$$W_{diss} = \pi h X^2 = \pi \eta k X^2 \tag{9}$$

This area, the integral of the force along the displacement, corresponds to the non-conservative work done per cycle. In other words, in a plot of force *vs* displacement at a given frequency, damping can be seen as a mechanism that introduces a lag between force and displacement and shows up as an elongated ellipse [19, 20]. In fact, from [21], it can be shown that the dissipated energy can be written in the alternative form:

$$W_{diss} = \pi F X \sin(\theta) \tag{10}$$

where θ is the phase angle between the force and the displacement response. From equations (9) and (10) a relationship between the hysteretic damping coefficient, the displacement, the force and the phase angle can be established as:

$$h = \frac{F}{X} sin(\theta) \tag{11}$$

For harmonic motion, the ratio between the force and the displacement is a transfer function often referred to as Dynamic Stiffness [1]. Usually, in experimentation, one measures the Receptance instead, which is the inverse of the Dynamic Stiffness. For harmonic motion, this is:

$$\alpha(\omega) = \frac{x(\omega)}{f(\omega)} \tag{12}$$

The quantities $x(\omega)$ and $f(\omega)$ are the complex response and complex force with amplitudes $X(\omega)$ and $F(\omega)$ respectively. If the amplitude of the receptance is represented by $H(\omega)$, then equation (11) can be re-written as:

$$\sin[\theta(\omega)] = h \cdot H(\omega) \tag{13}$$

The purpose of all this development was to write equation (13). This can be more simply written as:

$$\sin(\theta) = h \cdot H \tag{14}$$

if the dependency on the angular frequency is dropped for convenience.

This equation suggests that the hysteretic damping coefficient h can be simply determined from the measurement of the amplitude and phase of the receptance. The hysteretic damping factor η can then be determined from equation (7), but this requires that the stiffness k is known, which can be done, e.g., using the method of the inverse. The determination of the hysteretic damping factor from the damping coefficient following this method and the generalisation to multiple degree of freedom (MDOF) systems is addressed in detail in [9, 10].

If we plot equation (13) in a plane composed by the vertical axis $y \equiv \sin(\theta)$ and the horizontal axis $x \equiv H$, it should be clear that it resembles the equation of a straight line with slope h. However, it also has other important properties, discussed in the following sections.

2.3. Determination of the real and imaginary parts of the modal constant

The receptance (12) of an MDOF system can be expressed as [1]:

$$\alpha = \sum_{r=1}^{N} \frac{\bar{A}_r}{\omega_r^2 - \omega^2 + i\eta_r\omega_r^2} \tag{15}$$

where $\bar{A}_r$ and ω_r are the complex modal constant and angular natural frequency, respectively, for mode r, and N is the number of degrees of freedom (DOFs). If the modes are sufficiently spaced and at the vicinity of a resonance ω_r, the influence from other modes is small when compared to the resonant mode [9, 10]. Equation (15) becomes:

$$\alpha_{\omega\to\omega_r} \cong \frac{\bar{A}_r}{\omega_r^2 - \omega^2 + i\eta_r\omega_r^2} \tag{16}$$

which resembles the equation of an SDOF with a complex modal constant

$$\bar{A}_r = A_R + iA_I \tag{17}$$

where A_R and A_I are the real and imaginary parts of the modal constant, respectively. The whole following development is based on this assumption: that mode shapes are conveniently well spaced in the frequency spectrum so that equation (16) is true at the vicinity of mode r.

Condition 1: $|\omega_r^2 - \omega^2| \gg 0$

Away from the natural frequency, and considering, for better convenience, a lightly damped system where $\eta_r \cong 0$, equation (16) is simplified to:

$$\alpha_{\omega\ll\gg\omega_r} \cong \frac{A_R + iA_I}{\omega_r^2 - \omega^2} = \frac{A_R}{\omega_r^2 - \omega^2} + i\frac{A_I}{\omega_r^2 - \omega^2} \tag{18}$$

If the receptance is represented in the Argand plane, then the phase $\theta_{\omega\ll\gg\omega_r}$ is related to the imaginary $\alpha_{I_{\omega\ll\gg\omega_r}}$ and real $\alpha_{R_{\omega\ll\gg\omega_r}}$ parts of the receptance by:

$$\tan\left[\theta_{\omega\ll\gg\omega_r}\right] = \frac{\alpha_{I_{\omega\ll\gg\omega_r}}}{\alpha_{R_{\omega\ll\gg\omega_r}}} = \frac{\dfrac{A_I}{\omega_r^2 - \omega^2}}{\dfrac{A_R}{\omega_r^2 - \omega^2}} = \frac{A_I}{A_R} \tag{19}$$

and

$$\theta_{\omega\ll\gg\omega_r} = \tan^{-1}\left(\frac{A_I}{A_R}\right) \tag{20}$$

Therefore, in the $x \equiv H$ *vs* $y \equiv \sin(\theta)$ plane this becomes:

$$\sin\left[\theta_{\omega\ll\gg\omega_r}\right] = \sin\left[\tan^{-1}\left(\frac{\mathrm{A_I}}{\mathrm{A_R}}\right)\right] \tag{21}$$

Condition 2: $|\omega_r^2 - \omega^2| = 0$

When at the natural frequency, i.e., when $\omega = \omega_r$, equation (16) achieves its maximum value:

$$\alpha_{\omega=\omega_r} = \frac{A_R + iA_I}{i\eta_r\omega_r^2} = \frac{A_I}{\eta_r\omega_r^2} - i\frac{A_R}{\eta_r\omega_r^2} \tag{22}$$

Hence, the amplitude of the receptance

$$H = |\alpha| = \sqrt{\alpha_{Re}^2 + \alpha_{Im}^2} \tag{23}$$

at the resonance is:

$$H_{\omega=\omega_r} = \left|\alpha_{\omega=\omega_r}\right| = \frac{1}{\eta_r\omega_r^2}\sqrt{A_I^2 + A_R^2} \tag{24}$$

which, when solved for A_R, becomes:

$$A_R = \sqrt{H_{\omega=\omega_r}^2\eta_r^2\omega_r^4 - A_I^2} \tag{25}$$

Equation (25) allows determining the real part of the modal constant from its complex counterpart, which must be determined somehow. Therefore, if one solves equation (21) for A_I when having equation (25) in consideration, and after some mathematical manipulation, this results in:

$$A_I = \sqrt{\frac{H_{\omega=\omega_r}^2\eta_r^2\omega_r^4}{\left[\tan[\sin^{-1}(\theta_{\omega\ll\gg\omega_r})]\right]^{-2} + 1}} \tag{26}$$

Equations (25) and (26) allow determining the real and imaginary parts of the modal constant from the plot of the receptance in the $x \equiv H$ *vs* $y \equiv \sin(\theta)$ plane. For a matter of convenience, and as it will be better understood later, this will be henceforward referred to as 'elliptical plane'.

3. Properties of the receptance in the 'elliptical plane'

To illustrate how the representation of a receptance looks like in the 'elliptical plane' and how the modal constants are determined, let us first consider the example of an arbitrary SDOF system with complex modal constant $\bar{A}_r = 1000 + 500i$, 20.4 Hz natural frequency and a 1% modal damping factor. Let us also assume that the receptance was experimentally measured in the 0 to 40 Hz frequency range with a period of acquisition of 2 s (i.e., a 0.5 Hz frequency resolution). Plots of the amplitude H and phase θ of the receptance so obtained in the frequency domain and the same function in the 'elliptical plane' are shown in figures 1 and 2 respectively.

The procedure to determine the modal constants involved coding a software that does the following:

1. Representation of the receptance in the 'elliptical plane';
2. Extrapolation of the data points (near a resonant frequency) with an elliptical function centred at (0, 0) and tangent to an imaginary horizontal line at $y = \pm 1$;
3. Determination of $\theta_{\omega \ll \gg \omega_r}$ from the intersection of the ellipse at the y axis;
4. Determination of $H_{\omega=\omega_r}$ from the point where the ellipse is tangent to an imaginary vertical line;
5. Determination of the angle the ellipse makes with the horizontal to determine the hysteretic damping coefficient. The hysteretic damping factor is then determined in the same way to what was is done in [9, 10];
6. Determination of the modal constants from equations (25) and (26).

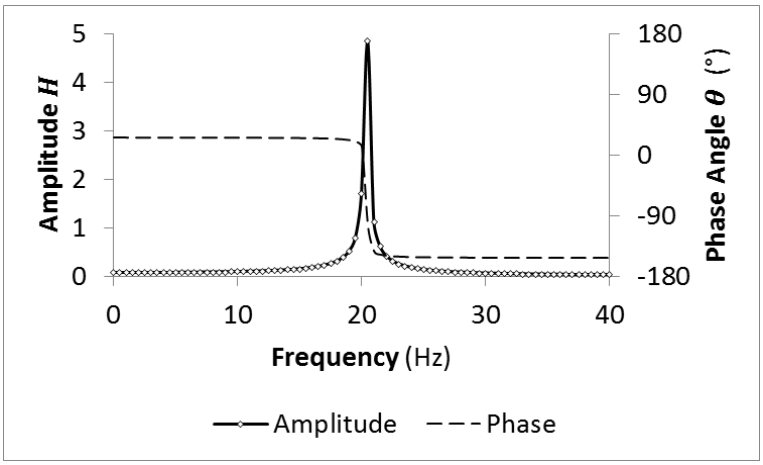

Figure 1. Numerical example of the amplitude and phase of a SDOF receptance in the frequency domain.

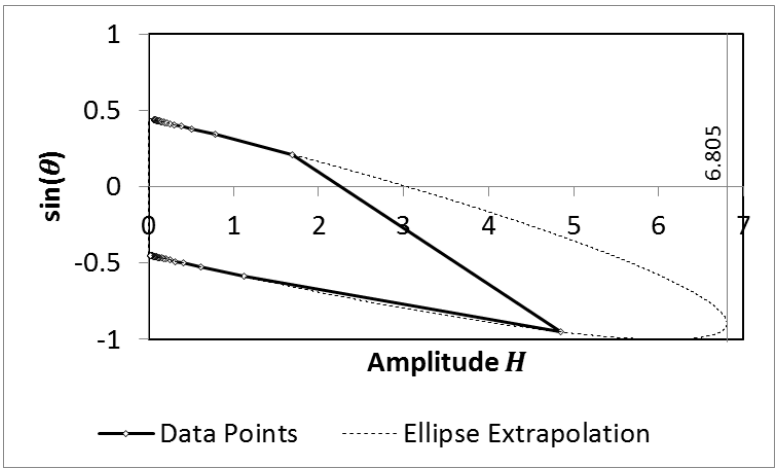

Figure 2. Numerical example of the same SDOF receptance represented in figure 1 in the 'elliptical plane'.

The first observation to note is that the receptance data points when plotted in the 'elliptical plane' describe a loop that can be fitted with the half of an ellipse. In this case, since the data has no noise and it is a SDOF, a perfect correlation between the data and the fit was obtained (figure 2). This ellipse has some important properties, namely:

1. The angle of the ellipse depends on the damping coefficient h and the ellipse is centred at (0, 0). This should not be a surprise, since equation (13) is the equation of a straight line with slope h, as observed before in [9, 10], and intercept at zero.

2. The function is limited between 1 and -1 since it depends on a sinusoidal trigonometric function. In the example shown, where half an ellipse is represented, the elliptical extrapolation is tangent at $y = -1$;
3. Since the natural frequency (20.4 Hz) is not a multiple of the frequency resolution (0.5 Hz) in the example shown, the frequency spectrum in figure 1 does not show the exact amplitude at the natural frequency (the maximum as seen from figure 1 would be 4.85). The amplitude at the resonance for this given example is determined to be 6.805 from equation (15) with $N = 1$ (since it is SDOF). At the same time, it can be observed from the given example that the ellipse in figure 2 is tangent at an imaginary vertical line that crosses the x axis at 6.805, precisely the amplitude at the resonance, $H_{\omega=\omega_r}$. This quantity is needed to determine the modal constants through equations (25) and (26). The advantage of the ellipse is that it allows determining the amplitude at the resonance from experimental data, whereas equation (15) would not be possible to use as starting point for most real situations;
4. The value $\theta_{\omega \ll \gg \omega_r}$ required to determine the imaginary part A_I of the modal constant (equation 26) can also be determined from the ellipse, since this is when the ellipse crosses the y axis, i.e. $\theta_{\omega \ll \gg \omega_r} = \sin^{-1}[\sin(\theta_{x=0})]$.

4. Numerical examples and results

A total of ten different cases were simulated to illustrate the proposed method. These are listed in table 1[†]. Cases 1 to 6 all are SDOF: cases 1 and 2 have real modal constants and cases 3 to 6 have complex modal constants with changing signals (as observed in [22] the signal of the modal constants is related to the signal of the slope of the ellipse major axis and the phase angle). Cases 7 and 8 are MDOF (2-DOF) with 'low' damping factors (figures 3 and 4) and cases 9 and 10 are MDOF with one 'highly damped' mode.

Figures 3 and 4 show the MDOF case 7 in both the frequency domain and 'elliptical plane', where the fitting ellipses can be clearly seen. However, the procedure assumes that the mode shapes are conveniently spaced, so that the influence from mode shapes at the vicinity of the mode shape being identified is as little as possible to be neglected. Therefore, each mode is identified individually by 'zooming-in' close to its respective natural frequency. This is shown in figures 5, 6, 7 and 8 where the receptance near the first and second mode shapes are represented, respectively, in the frequency domain (amplitude and phase) and in the 'elliptical plane'.

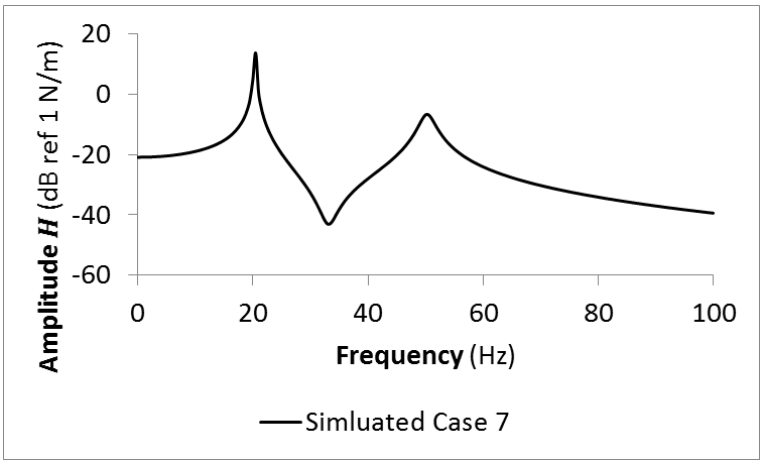

Figure 3. Amplitude of the MDOF receptance for numerical case 7 in the frequency domain.

[†] The modal constants, natural frequencies and hysteretic damping factors may not have any physical/real meaning. They were chosen for the specific purpose of the demonstration.

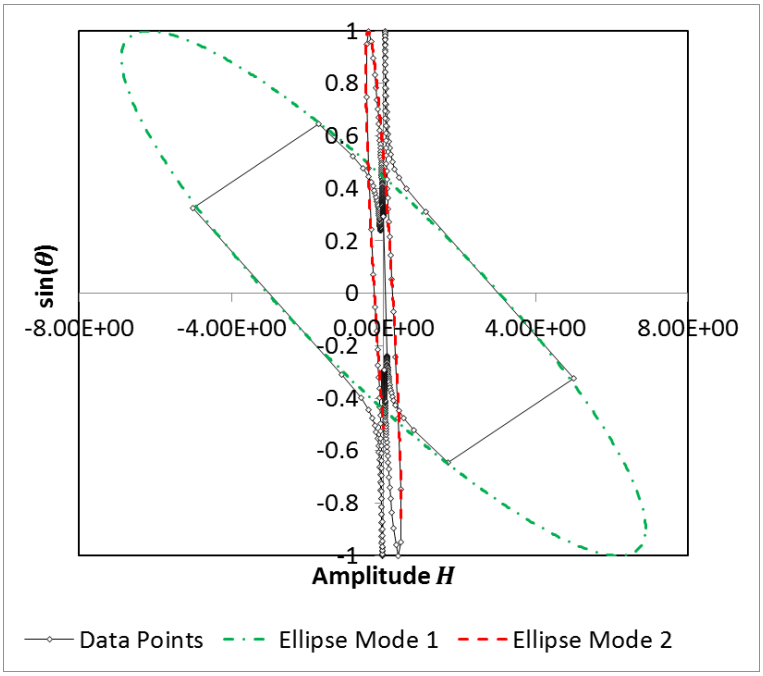

Figure 4. MDOF receptance for numerical case 7 (figure 3) represented in the 'elliptical plane' with two ellipses fitting the date at the vicinity of the mode shapes (the plot was mirrored for better convenience. Only half of the ellipse is actually visible with the discussed method).

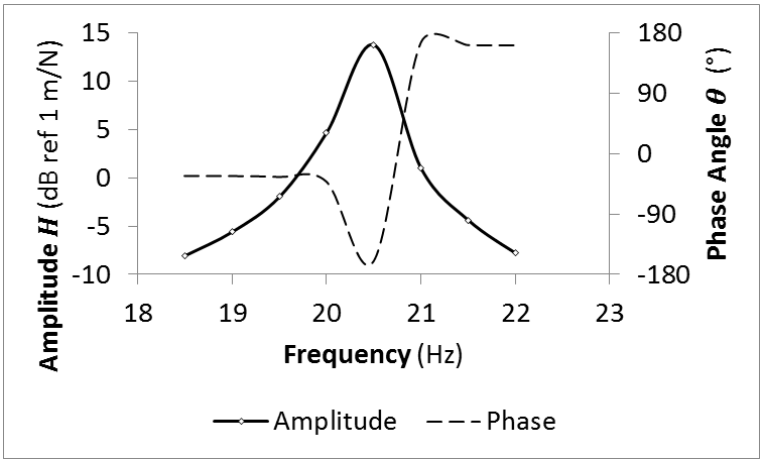

Figure 5. Amplitude and phase of the receptance in the frequency domain near the 1st resonance of simulated case 7.

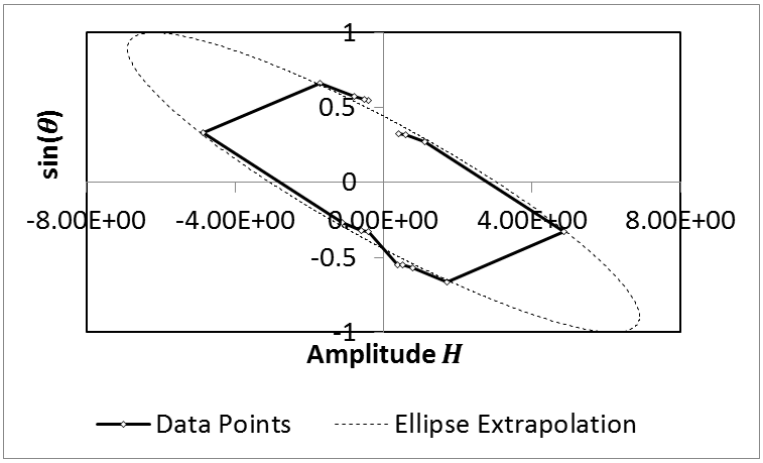

Figure 6. Receptance near the 1st resonance of simulated case 7 (represented in the 'elliptical plane') with the modal identification fitting ellipse (the plot was mirrored for better convenience).

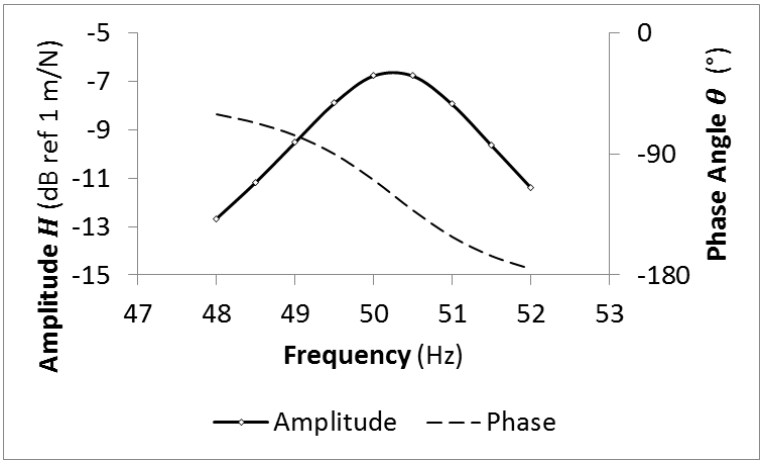

Figure 7. Amplitude and phase of the receptance in the frequency domain near the 2nd resonance of simulated case 7.

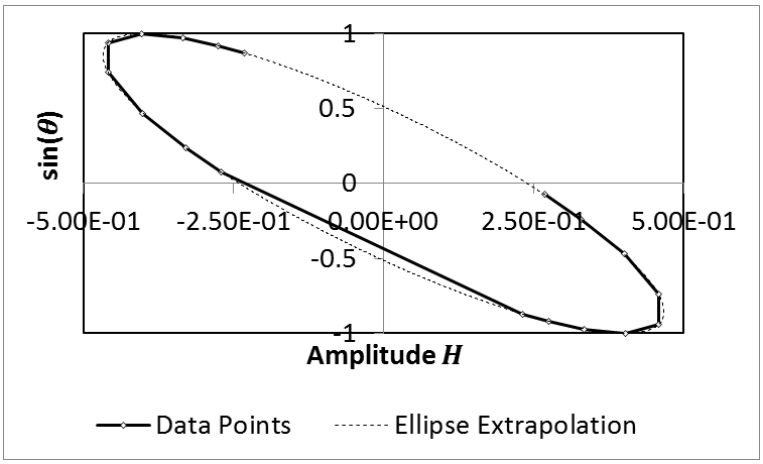

Figure 8. Receptance near the 2nd resonance of simulated case 7 (represented in the 'elliptical plane') with the modal identification fitting ellipse (the plot was mirrored for better convenience).

The results from the modal identification following the process described herewith are shown in table 2. The percent difference between the theoretical values (table 1) and the numerical results (table 2) are presented in table 3.

Table 1. Numerical models' theoretical properties.

	Mode 1					Mode 2				
	Modal Constant 1		f (Hz)	η (%)	Amp	Modal Constant 2		f (Hz)	η (%)	Amp
Case	Real	Imag				Real	Imag			
1	1000	0	20.4	1	6.087	-	-	-	-	-
2	-1000	0	20.4	1	6.087	-	-	-	-	-
3	1000	500	20.4	1	6.805	-	-	-	-	-
4	-1000	-500	20.4	1	6.805	-	-	-	-	-
5	1000	-500	20.4	1	6.805	-	-	-	-	-
6	-1000	500	20.4	1	6.805	-	-	-	-	-
7	1000	-500	20.4	1	6.805	2000	-1200	50.25	5	0.4679
8	1000	-500	20.4	1	6.805	2000	1200	50.25	5	0.4679
9	1000	-500	20.4	1	6.805	2000	-1200	50.25	50	0.04679
10	1000	-500	20.4	50	0.1361	2000	-1200	50.25	5	0.4679

Table 2. Results from the modal identification (numerical examples).

	Mode 1					Mode 2				
	Modal Constant 1		f (Hz)	η (%)	Amp	Modal Constant 2		f (Hz)	η (%)	Amp
Case	Real	Imag				Real	Imag			
1	1041	1.033	20.4	1	6.203	-	-	-	-	-
2	-1000	1.013	20.4	1	6.087	-	-	-	-	-
3	1000	500	20.4	1	6.805	-	-	-	-	-
4	-1000	-500	20.4	1	6.805	-	-	-	-	-
5	1000	-500	20.4	1	6.805	-	-	-	-	-
6	-1000	500	20.4	1	6.805	-	-	-	-	-
7	1016	-502.1	20.4	1	6.892	2001	-1198	50.25	5.003	0.4676
8	1000	-500	20.4	1	6.799	2000	1200	50.25	5	0.4679
9	993.8	-520.3	20.4	1.027	6.648	2021	-1201	50.29	49.92	0.04715
10	995.1	-502.1	20.4	50.16	0.1353	1996	-1208	50.25	4.979	0.4700

Table 3. Difference between the theoretical values and the numerical results (all values are expressed in %).

	% error mode 1					% error mode 2				
	Modal Constant 1		f	η	Amp	Modal Constant 2		f	η	Amp
Case	Real	Imag				Real	Imag			
1	4.10	-	0.00	0.00	1.91	-	-	-	-	-
2	0.00	-	0.00	0.00	0.00	-	-	-	-	-
3	0.00	0.00	0.00	0.00	0.00	-	-	-	-	-
4	0.00	0.00	0.00	0.00	0.00	-	-	-	-	-
5	0.00	0.00	0.00	0.00	0.00	-	-	-	-	-
6	0.00	0.00	0.00	0.00	0.00	-	-	-	-	-
7	1.60	0.42	0.00	0.00	1.28	0.05	-0.17	0.00	0.06	-0.06
8	0.00	0.00	0.00	0.00	-0.09	0.00	0.00	0.00	0.00	0.00
9	-0.62	4.06	0.00	2.70	-2.31	1.05	0.08	0.08	-0.16	0.77
10	-0.49	0.42	0.00	0.32	-0.59	-0.20	0.67	0.00	-0.42	0.45

Table 3 shows that there is good agreement between the theoretical models and the results obtained from the modal identification, at least for SDOF systems. The MDOF produced slightly worse results, but still acceptable. The worst cases were cases 1, 9 and 10. In the 'ideal' case 1, where the modal constant is real, the ellipse becomes a straight line, hence the identification process fails due to problems related to the ellipse curve fitting (i.e., the ellipse has no minor axis). Hence, a small value had to be determined to the imaginary part of the modal constant so that the algorithm produced meaningful results. Nevertheless, in real situations, the modal constants normally are complex quantities, therefore this 'ideal' situation might not represent a real issue. Regarding cases 9 and 10, the slightly higher errors

may be related to the presence of a 'highly damped' mode shape. Since the method was developed for lightly damped systems, this result is not surprising. Even though, the maximum error was in the identification of the imaginary part of the first modal constant with a value of 4.1% only.

It is important to note that the modal identification process 'isolated' the mode shapes as suggested in [22, 23], with the aim to improve the modal parameters' identification accuracy. This technique exists in other modal identification methods, for example in the BetaLAB software [23] that makes use of the Characteristic Response Function (CRF) [24]. In this technique, once one mode shape is identified, it is subtracted from the experimental curve to eliminate (or at least reduce) the influence from other mode shapes. This also means that the modal identification process is run at least twice so that each mode is identified with the minimum possible influence from the other mode shapes in the frequency range.

5. Experimental examples and results

5.1. *Validation of experimental results*

Experimental vibration data from a carbon fibre rectangular plate suspended in a free-free simulated configuration (as described in section 5.2 below) was used to better assess the performance of the proposed method. The results were then compared with the ones obtained using BetaLAB, a modal identification software developed in [23] that makes use of the CRF [24]. The reason why another method was used concurrently was to get a benchmark set of values, since experimental modal properties are not known beforehand for comparison. Therefore, the performance of BetaLAB was also assessed using the numerical cases 7 to 10 described in table 1 and available from section 4. Results are presented in tables 4 and 5.

Table 4. Results from the modal identification using BetaLAB (numerical examples).

	Mode 1					Mode 2				
	Modal Constant 1		f (Hz)	η (%)	Amp	Modal Constant 2		f (Hz)	η (%)	Amp
Case	Real	Imag				Real	Imag			
7	1003	-502.5	20.4	1.001	6.821	1999	-1200	50.25	4.999	0.4679
8	999.8	-499.8	20.4	0.9995	6.807	2049	1187	50.25	5.054	0.4700
9	999.0	-505.3	20.4	0.9980	6.828	1994	-1205	50.27	49.95	0.04675
10	1027.0	-514.0	20.3	51.37	0.137	1999	-1200	50.25	5.001	0.4677

Table 5. Difference between the theoretical values and the numerical results from BetaLAB (all values are expressed in %).

	% error mode 1					% error mode 2				
	Modal Constant 1		f	η	Amp	Modal Constant 2		f	η	Amp
Case	Real	Imag				Real	Imag			
7	0.30	0.50	0.00	0.10	0.24	-0.05	0.00	0.00	-0.02	-0.01
8	-0.02	-0.04	0.00	-0.05	0.03	2.45	-1.08	0.00	1.08	0.45
9	-0.10	1.06	0.00	-0.20	0.34	-0.30	0.42	0.04	-0.10	-0.08
10	2.70	2.80	-0.49	2.74	0.97	-0.05	0.00	0.00	0.02	-0.05

The most important conclusion is that both methods agree quite well with the numerical results. They also seem to be equivalent in terms of performance, at least with the numerical results provided. The maximum percent differences between these results and the theoretical values for the modal constants is 2.80% (BetaLAB) and 4.06% (method of the Ellipse). However, on average, these differences reduce to 0.74% and 0.61%, respectively. Regarding the modal damping factors, the maximum percent differences are 2.74% (BetaLAB) and 2.70% (method of the Ellipse), but the average differences are 0.54% and 0.46, respectively. Since the maximum percent differences do not apply to the same cases and/or mode shapes, plus the average differences are essentially the same and very small, it is very difficult to find a better explanation rather than one that is based on numerical uncertainty/ill-conditioning and human error. It is important to note that both BetaLAB and the method of the Ellipse

rely, up to a certain extent, on the user's judgment. This also means that it is unlikely that two modal identifications on the same data points will ever produce the exact same results when either of the software is used.

5.2. *Experimental setup*

The composite plate used in this study is formed by 8 unidirectional layers with a $[0/90]_{2S}$ layup. Each layer is made of an epoxy resin impregnated with carbon fibre satin weave Cytec Cycom 934-373KT300. The dimensions of the test plate are, approximately, 360x262x3mm.

Free-free boundary conditions were simulated in the lab. The specimen plate was suspended vertically by 2 nylon strings, which were attached to two 1mm diameter drilled holes positioned at a distance of 50mm from the plate's sides and at 5mm from its top edge. A transfer Frequency Response Function (FRF) were measured using a National Instruments DAQ-9234 analogue input data acquisition module on a National Instruments cDAQ-9174 USB chassis. The first channel was allocated to the excitation force (measured with a PCB 208C01 force transducer) and the other one was used to measure the acceleration response with a PCB 352C22 lightweight teardrop accelerometer.

An electromagnetic shaker LDS V201 was used to produce the excitation signal, at a single coordinate, with a copper pushrod 60mm long attached to the force transducer at the other end. A multisine [25] excitation signal ranging from 0 to 200Hz with a 0.25 Hz frequency resolution was generated and amplified using a NI 9263 analogue output module and an LDS PA25E power amplifier.

Signal Express 2012 from National Instruments was used to process and record the results. The FRFs were recorded under the form of Receptance and a Rectangular window was used during the signal acquisition.

5.3. *Results*

The experimental receptance plot, as well as the regenerated curves from the modal identification with both the method of the Ellipse and BetaLAB, are shown in figure 9. As with the numerical examples, each mode is identified individually by 'zooming-in' close to its respective natural frequency, so that the influence from mode shapes at the vicinity of the mode shape being identified is as little as possible. This is shown in figures 10-17 where the receptances near the four mode shapes are represented, respectively, in the frequency domain (amplitude and phase) and in the 'elliptical plane'.

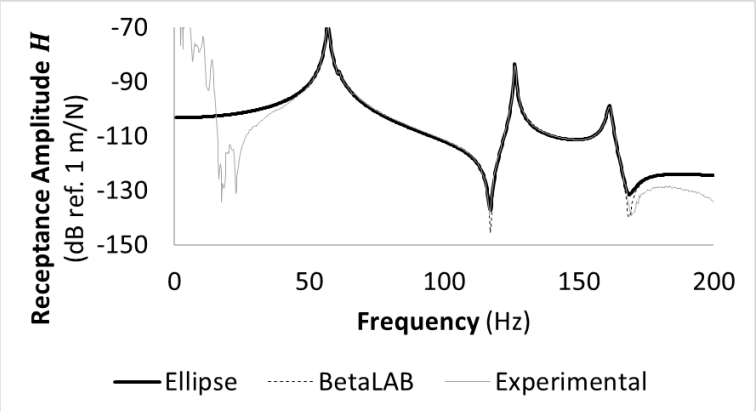

Figure 9. Receptance curve in the 0 to 200 Hz frequency range – experimental curve and regenerated identified curves through the method of the Ellipse and the software BetaLAB.

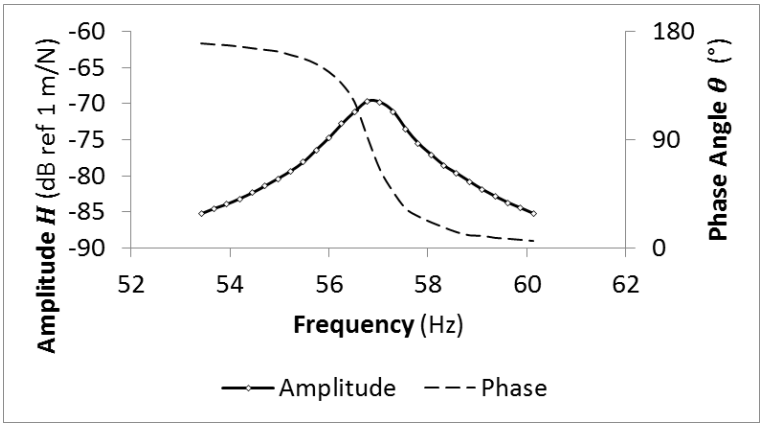

Figure 10. Amplitude and phase of the receptance in the frequency domain near the 1st experimental resonance.

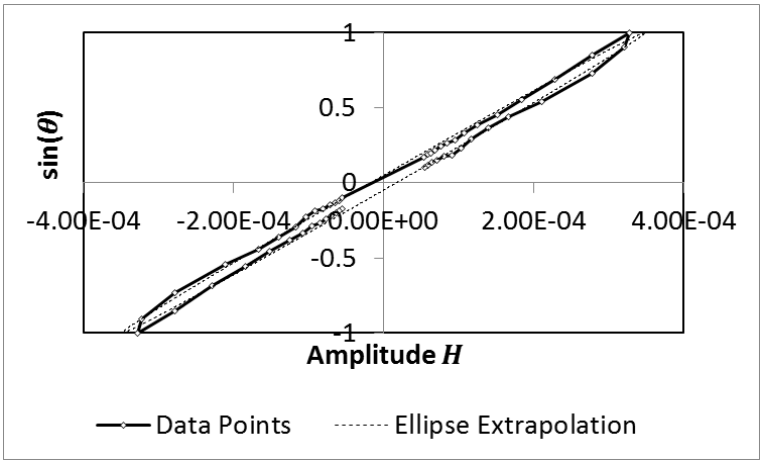

Figure 11. Receptance near the 1st experimental resonance (represented in the 'elliptical plane') with the modal identification fitting ellipse (the plot was mirrored for better convenience).

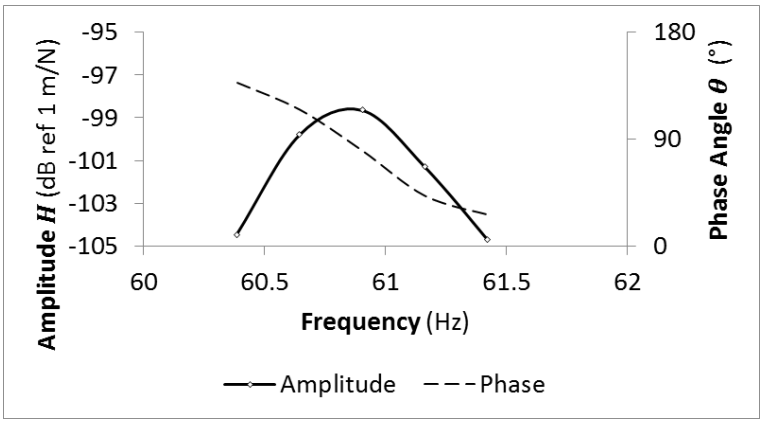

Figure 12. Amplitude and phase of the receptance in the frequency domain near the 2nd experimental resonance.

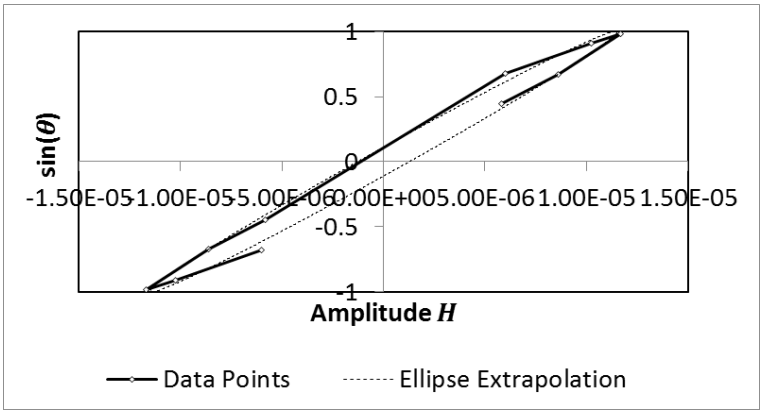

Figure 13. Receptance near the 2nd experimental resonance (represented in the 'elliptical plane') with the modal identification fitting ellipse (the plot was mirrored for better convenience).

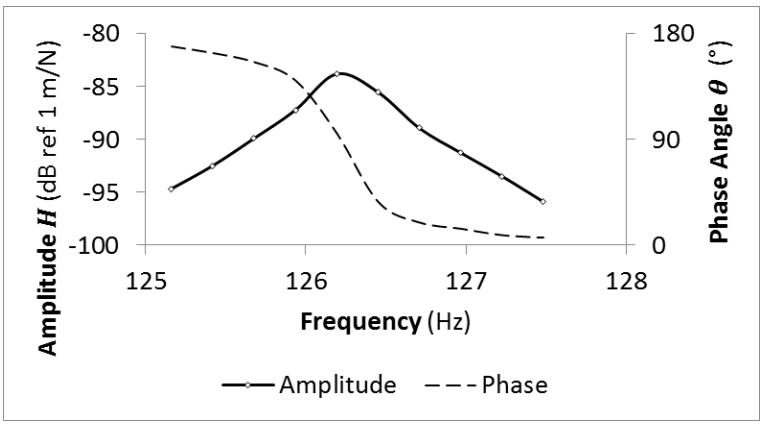

Figure 14. Amplitude and phase of the receptance in the frequency domain near the 3rd experimental resonance.

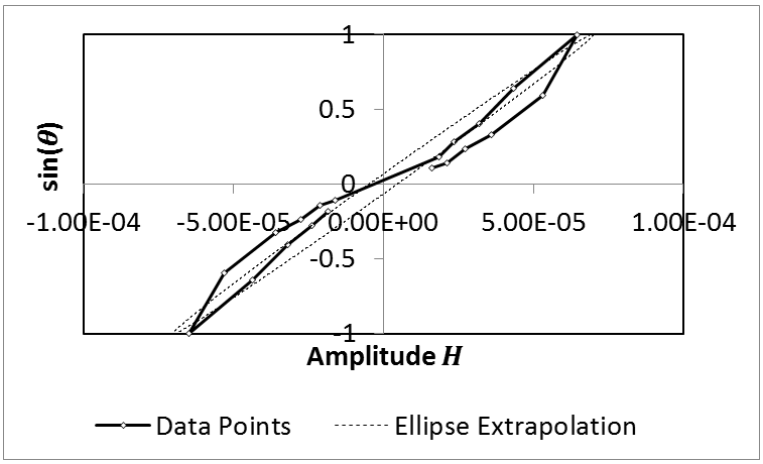

Figure 15. Receptance near the 3rd experimental resonance (represented in the 'elliptical plane') with the modal identification fitting ellipse (the plot was mirrored for better convenience).

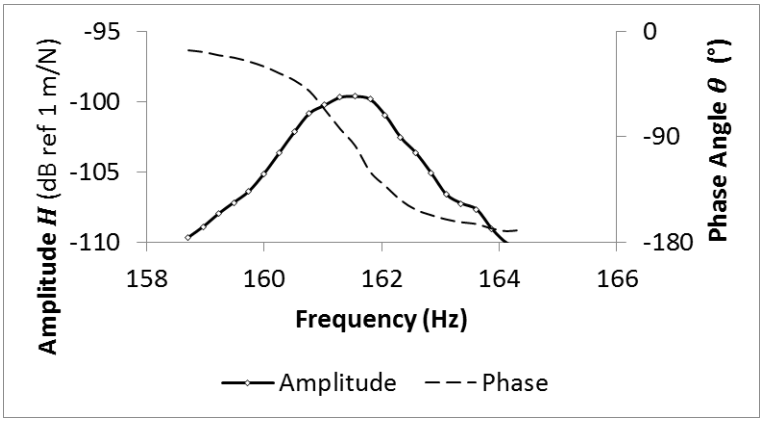

Figure 16. Amplitude and phase of the receptance in the frequency domain near the 4th experimental resonance.

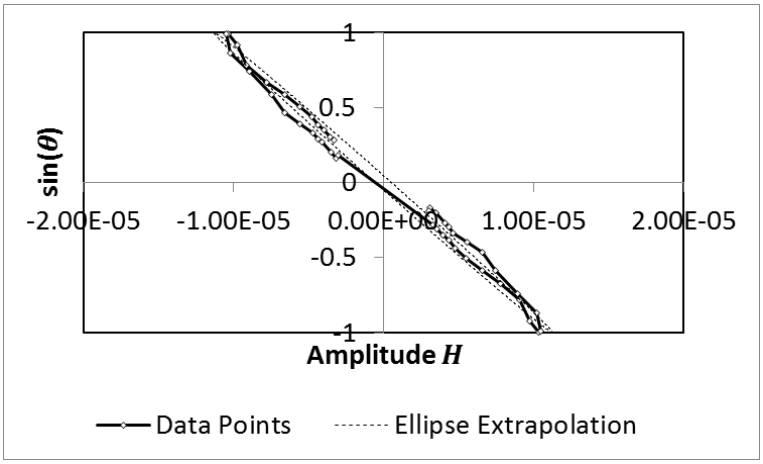

Figure 17. Receptance near the 4th experimental resonance (represented in the 'elliptical plane') with the modal identification fitting ellipse (the plot was mirrored for better convenience).

The percent difference between the values obtained with the method of the Ellipse (table 6) and BetaLAB (table 7) are presented in table 8. It is important to mention that, because experimental data has noise, the 'best ellipse fitting' was determined by a combination of two parameters: a correlation factor (based on a least-squares fit) and the best approximation between the area of the shape formed by the data points in the 'elliptical plane' and the extrapolated ellipse.

Table 6. Results from the modal identification using the method of the Ellipse (experimental examples).

	Identification from Method of the Ellipse			
	Modal Constants		η (%)	Amp
Mode	Real	Imag		
1	-8.243E-01	4.522E-02	1.866	3.470E-04
2	-1.808E-02	3.504E-03	1.051	1.199E-05
3	-2.033E-01	1.171E-02	0.4551	7.118E-05
4	1.155E-01	6.039E-03	0.996	1.121E-05

Table 7. Results from the modal identification using the software BetaLAB (experimental examples).

	Identification from BetaLAB			
	Modal Constants		η (%)	Amp
Mode	Real	Imag		
1	-8.285E-01	4.077E-02	1.876	3.464E-04
2	-1.674E-02	-7.510E-04	0.9793	1.172E-05
3	-1.976E-01	7.004E-03	0.4401	7.143E-05
4	1.148E-01	-8.384E-03	0.9959	1.124E-05

Table 8. Difference between the results obtained with the method of the Ellipse and the software BetaLAB (all values are expressed in %).

	% difference between Ellipse and BetaLAB			
	Modal Constants		η	Amp
Mode	Real	Imag		
1	0.12	-0.05	-0.35	0.52
2	4.68	-396	5.90	-0.76
3	1.55	92.4	3.89	-2.10
4	0.04	-165	-0.45	0.42

Results from table 8 show that, in general, there is good agreement between the method of the Ellipse and BetaLAB with respect to the real part of the modal constants, the hysteretic damping factor and the amplitude of the receptance. This is also true for the second mode shape (figures 12 and 13) which is barely visible in the receptance figure 9. However, the same cannot be said to the imaginary part of the modal constants, which differ significantly from one method to the other, both in terms of amplitude and sign. This may well be due to the values being one to two orders of magnitude smaller than their real counterparts, reason why it does not seem to affect too much the regenerated curves[‡] shown in figure 9.

6. Conclusions

A novel method for the identification of the modal constants from FRFs, based on the dissipated energy per vibration cycle, was presented. It is mostly suitable for lightly damped systems with conveniently spaced mode shapes. However, and more importantly, it offers an alternative way to represent the receptance, in a so-called 'elliptical plane'. The authors believe this may bring valuable insights for other researchers in the field. For example, since the elliptical shape of the receptance (in the vicinity of a resonant frequency) when represented in the 'elliptical plane' depends on both local and global modal properties, then it is reasonable to assume that this representation of the FRF can be used in other fields, such as Structural Health Monitoring.

In previous works [9, 10], it was shown that this method can provide a better estimate of the modal damping factors than the method of the inverse. By "isolating" the already identified mode shapes to reduce the degree of influence from the other mode shapes, the results agree quite well with the ones from BetaLAB. However, with respect to the modal constants, namely their imaginary parts, more research is still required, although the discrepancies between the results did not seem to visibly affect the regeneration of the identified curves. Furthermore, this may well be due to the imaginary parts of the modal constants being one to two orders of magnitude smaller than their real counterparts, hence being more prone to uncertainty and error.

Finally, although the method has not been tested on the modal identification of multiple FRF functions, this should not be a real issue. The challenges are mostly related with software implementation rather than with the method itself, since the representation of the receptance in the 'elliptical plane' greatly

[‡] Residuals, which are usually included to account for the influence of modes outside the measured frequency range, were not determined in this study.

depends on local properties. Consistency conditions between the modal constants to satisfy orthogonality properties between the eigenvectors can be implemented at a later stage, in the same way to what is done in [24].

Acknowledgements

The authors gratefully acknowledge the Niger Delta Development Commission for the financial support to this research work through grant NDDC/DEHSS/2015PGFS/RVS/025/30.

References

1. Maia, N.M.M. and J.M.M. e Silva, *Theoretical and experimental modal analysis*. 1997: Research Studies Press Taunton.
2. Au, S.-K., *Uncertainty law in ambient modal identification---Part II: Implication and field verification.* Mechanical systems and signal processing, 2014. **48**(1–2): p. 34-48.
3. Cheng, L. and D. Zheng, *The identification of a dam's modal parameters under random support excitation based on the Hankel matrix joint approximate diagonalization technique.* Mechanical systems and signal processing, 2014. **42**(1–2): p. 42-57.
4. Le, T.-P. and P. Paultre, *Modal identification based on the time–frequency domain decomposition of unknown-input dynamic tests.* International Journal of Mechanical Sciences, 2013. **71**: p. 41-50.
5. Sadhu, A., B. Hazra, and S. Narasimhan, *Decentralized modal identification of structures using parallel factor decomposition and sparse blind source separation.* Mechanical systems and signal processing, 2013. **41**(1–2): p. 396-419.
6. Gonilha, J.A., et al., *Modal identification of a GFRP-concrete hybrid footbridge prototype: Experimental tests and analytical and numerical simulations.* Composite Structures, 2013. **106**: p. 724-733.
7. Zapico-Valle, J.L., M. García-Diéguez, and R. Alonso-Camblor, *Nonlinear modal identification of a steel frame.* Engineering Structures, 2013. **56**: p. 246-259.
8. Zhang, L. and R. Brincker. *An overview of operational modal analysis: major development and issues*. in *1st International Operational Modal Analysis Conference*. 2005. Copenhagen, Denmark.
9. Montalvão, D. and J.M.M. Silva. *A contribution to the modal identification of the damping factor based on the dissipated energy*. in *EURODYN 2014 - IX International Conference on Structural Dynamics*. 2014. Porto, Portugal.
10. Montalvão, D. and J.M.M. Silva, *An alternative method to the identification of the modal damping factor based on the dissipated energy.* Mechanical Systems and Signal Processing, 2015. **54–55**: p. 108-123.
11. Silva, J., N. Maia, and A. Ribeiro. *Modal Constants Consistency: Application of a New Method for Solving Overdetermined Non-linear Equations*. in *Proceedings of the 12th International Modal Analysis Conference (XII IMAC)*. 1994. Honolulu, Hawai.
12. Allemang, R.J., *The modal assurance criterion–twenty years of use and abuse.* Sound and vibration, 2003. **37**(8): p. 14-23.
13. Devriendt, C. and P. Guillaume, *Identification of modal parameters from transmissibility measurements.* Journal of Sound and Vibration, 2008. **314**(1): p. 343-356.
14. Ewins, D.J., *Modal testing: theory and practice*. 1984, Letchworth, England: Research studies press.
15. Montalvao, D., N.M.M. Maia, and A.M.R. Ribeiro, *A review of vibration-based structural health monitoring with special emphasis on composite materials.* Shock and Vibration Digest, 2006. **38**(4): p. 295-326.
16. Ribeiro, A., J. Silva, and N. Maia, *On the generalisation of the transmissibility concept.* Mechanical Systems and Signal Processing, 2000. **14**(1): p. 29-35.

17. Silva, J., N. Maia, and A. Ribeiro, *Cancellation of mass-loading effects of transducers and evaluation of unmeasured frequency response functions.* Journal of Sound and Vibration, 2000. **236**(5): p. 761-779.
18. Sohn, H., et al., *A review of structural health review of structural health monitoring literature 1996-2001*. 2002, Los Alamos National Laboratory.
19. Lazan, B.J., *Damping of materials and members in structural mechanics*. 1968, Oxford, England: Pergamon Press Ltd.
20. Montalvão, D., et al., *Experimental measurement of the complex Young's modulus on a CFRP laminate considering the constant hysteretic damping model.* Composite Structures, 2013. **97**: p. 91-98.
21. Meirovitch, L., *Elements of vibration analysis*. 1975, New York, United States: McGraw-Hill.
22. Montalvão, D., D. Amafabia, and J. Silva. *And yet another method for the identification of modal constants in experimental modal analysis*. in *Proceedings of the 7th International Operational Modal Analysis Conference (IOMAC 2017)*. 2017. Ingolstadt, Germany.
23. Montalvão, D., *A modal-based contribution to damage location in laminated composite plates*, in *Mechanical Engineering Department*. 2010, PhD dissertation, Instituto Superior Técnico, Technical University of Lisbon.
24. Silva, J., N. Maia, and A. Ribeiro, *Structural dynamic identification with modal constant consistency using the characteristic response function (CRF).* Machine Vibration, 1996. **5**(2): p. 83-88.
25. Guillaume, P., et al. *Multisine excitations- new developments and applications in modal analysis*. in *Proceedings of the 19th International Modal Analysis Conference (IMAC XIX)*. 2001. Orlando, Kissimmee, FL.

FIGURE CAPTIONS

Figure 1. Numerical example of the amplitude and phase of a SDOF receptance in the frequency domain.

Figure 2. Numerical example of the same SDOF receptance represented in figure 1 in the 'elliptical plane'.

Figure 3. Amplitude of the MDOF receptance for numerical case 7 in the frequency domain.

Figure 4. MDOF receptance for numerical case 7 (figure 3) represented in the 'elliptical plane' with two ellipses fitting the date at the vicinity of the mode shapes (the plot was mirrored for better convenience. Only half of the ellipse is actually visible with the discussed method).

Figure 5. Amplitude and phase of the receptance in the frequency domain near the 1st resonance of simulated case 7.

Figure 6. Receptance near the 1st resonance of simulated case 7 (represented in the 'elliptical plane') with the modal identification fitting ellipse (the plot was mirrored for better convenience).

Figure 7. Amplitude and phase of the receptance in the frequency domain near the 2nd resonance of simulated case 7.

Figure 8. Receptance near the 2nd resonance of simulated case 7 (represented in the 'elliptical plane') with the modal identification fitting ellipse (the plot was mirrored for better convenience).

Figure 9. Receptance curve in the 0 to 200 Hz frequency range – experimental curve and regenerated identified curves through the method of the Ellipse and the software BetaLAB.

Figure 10. Amplitude and phase of the receptance in the frequency domain near the 1st experimental resonance.

Figure 11. Receptance near the 1st experimental resonance (represented in the 'elliptical plane') with the modal identification fitting ellipse (the plot was mirrored for better convenience).

Figure 12. Amplitude and phase of the receptance in the frequency domain near the 2nd experimental resonance.

Figure 13. Receptance near the 2nd experimental resonance (represented in the 'elliptical plane') with the modal identification fitting ellipse (the plot was mirrored for better convenience).

Figure 14. Amplitude and phase of the receptance in the frequency domain near the 3rd experimental resonance.

Figure 15. Receptance near the 3rd experimental resonance (represented in the 'elliptical plane') with the modal identification fitting ellipse (the plot was mirrored for better convenience).

Figure 16. Amplitude and phase of the receptance in the frequency domain near the 4th experimental resonance.

Figure 17. Receptance near the 4th experimental resonance (represented in the 'elliptical plane') with the modal identification fitting ellipse (the plot was mirrored for better convenience).

TABLE CAPTIONS

Table 1. Numerical models' theoretical properties.

Table 2. Results from the modal identification (numerical examples).

Table 3. Difference between the theoretical values and the numerical results (all values are expressed in %).

Table 4. Results from the modal identification using BetaLAB (numerical examples).

Table 5. Difference between the theoretical values and the numerical results from BetaLAB (all values are expressed in %).

Table 6. Results from the modal identification using the method of the Ellipse (experimental examples).

Table 7. Results from the modal identification using the software BetaLAB (experimental examples).

Table 8. Difference between the results obtained with the method of the Ellipse and the software BetaLAB (all values are expressed in %).